

LASER INTERFEROMETER GRAVITATIONAL WAVE OBSERVATORY
- LIGO -
CALIFORNIA INSTITUTE OF TECHNOLOGY
MASSACHUSETTS INSTITUTE OF TECHNOLOGY

Engineering Note	LIGO-E1500247-v1	2015/08/03
LIGO SURF Progress Report 2: Investigation of Thermal Noise in Thin Silicon Structures		
Matthew Winchester Mentors: Nicolas Smith, Zach Korth, Rana Adhikari		

California Institute of Technology
LIGO Project, MS 18-34
Pasadena, CA 91125
Phone (626) 395-2129
Fax (626) 304-9834
E-mail: info@ligo.caltech.edu

Massachusetts Institute of Technology
LIGO Project, Room NW22-295
Cambridge, MA 02139
Phone (617) 253-4824
Fax (617) 253-7014
E-mail: info@ligo.mit.edu

LIGO Hanford Observatory
Route 10, Mile Marker 2
Richland, WA 99352
Phone (509) 372-8106
Fax (509) 372-8137
E-mail: info@ligo.caltech.edu

LIGO Livingston Observatory
19100 LIGO Lane
Livingston, LA 70754
Phone (225) 686-3100
Fax (225) 686-7189
E-mail: info@ligo.caltech.edu

Contents

1	Introduction	2
2	Driven, Damped Oscillators	3
3	Internal Damping	4
4	Experimental Setup	5
5	Cantilever Designs	6
6	Measurement Techniques	8
6.1	Ringdown Method	8
6.2	Continuous Method	9
7	Mechanical Losses in Silicon	11
7.1	Thermoelastic Loss	11
7.2	Clamp Design and Clamp Loss Simulations	13
7.3	Surface Loss	15
8	Future Work	16

Abstract

Current aLIGO (Advanced Laser Interferometer Gravitational-Wave Observatory) suspensions and test masses are built from a fused silica substrate. In an effort to further increase detector sensitivity in the mid LIGO frequency band, which is currently limited by thermal noise, cryogenic silicon has become a candidate for the next generation of detector suspensions and test masses due to its excellent mechanical and optical properties. The fluctuation-dissipation theorem links microscopic thermal noise fluctuations with macroscopic material damping, which in turn motivates the study of damping mechanisms in silicon structures. In this project we demonstrate and assess several methods for measuring the quality factor of silicon cantilevers, including a continuous measurement technique capable of measuring the quality factor of several resonant modes simultaneously. We also investigate the effects of parameters such as temperature, cantilever geometry, and surface treatments on the quality factor with the goal of informing future detector suspension designs.

1 Introduction

LIGO (Laser Interferometer Gravitational-Wave Observatory) is a massive physics experiment designed to detect gravitational waves originally predicted by Einstein's general theory of relativity in 1916. Each detector is essentially a Michelson interferometer. As gravitational waves pass through the detectors, they distort local space-time and change the effective path length difference between the two perpendicular arms of the interferometer. This creates a relative phase shift between the two beams and allows for constructive interference at the photodiode detector, resulting in a measureable signal that indicates the presence of gravitational waves. Two independent detectors have been built and operated in Livingston, Louisiana and Hanford, Washington. The second generation of LIGO detectors, Advanced LIGO (aLIGO), have been constructed and are currently being commissioned to optimize sensitivity. The first data run of aLIGO is scheduled to begin in Fall 2015.

Research has already begun concerning the third generation of LIGO detectors. There are many different sources of noise that limit the precision of the experiment, such as shot noise, seismic vibrations, and thermal noise. In the frequency band relevant for the detection of gravitational waves (10-100Hz), thermal noise in the test masses and suspensions is currently a major factor limiting precision. The aLIGO test masses and suspensions are made of a fused silica material. Cryogenic silicon is now being considered as an alternative construction material for the next generation of LIGO detectors in order to further reduce thermal noise and increase sensitivity in the low frequency band of interest [1].

Thermal noise can be very difficult to measure directly. However, the fluctuation-dissipation theorem relates the dissipation of a perturbed system to the thermal fluctuations of the system at equilibrium. This means that the mechanical dissipation of the material can be studied instead, and this is usually a much easier approach in practice. Previous work has been done investigating the quality factor of thin silicon flexures through ringdown measurement techniques [2, 3]. This project focuses on both ringdown measurements and more advanced techniques such as continuous measurements using feedback control loops.

2 Driven, Damped Oscillators

An externally driven oscillator with linear damping is most commonly modeled as the differential equation:

$$m\ddot{x} + b\dot{x} + kx = f_{ext} \quad (1)$$

where m is the mass of the oscillator, b is the damping coefficient, and k is the restorative spring constant. This differential equation is easy to solve in the frequency domain by taking the Laplace transform:

$$ms^2X(s) + bsX(s) + kX(s) = F_{ext}(s) \quad (2)$$

The transfer function of the system is defined as the ratio of $X(s)/F_{ext}(s)$:

$$H(s) = \frac{X(s)}{F_{ext}(s)} = \frac{1}{ms^2 + bs + k} \quad (3)$$

The system acts as a second order low pass filter. Our resonators have very small dissipation, so we focus on the case of underdamped motion, where $b^2/4km \ll 1$. It is also convenient to introduce the three terms $\gamma = b/m$ (damping ratio), $\omega_0 = \sqrt{k/m}$ (natural frequency), and $\tau = 2/\gamma$ (characteristic time). In this regime, the two poles of the transfer function are at:

$$s = \frac{-\gamma}{2} \pm i\sqrt{\omega_0^2 - \gamma^2/4} \quad (4)$$

The maximum value of $|H(i\omega)|$ is at the frequency $\omega_{max} = \sqrt{\omega_0^2 - \gamma^2/2}$. Taking the same underdamped limit above, the γ^2 term is negligible so $\omega_{max} \approx \omega_0$. A plot of the transfer function with normalized frequency is shown in Figure 1 below, with $\gamma = 0.05$:

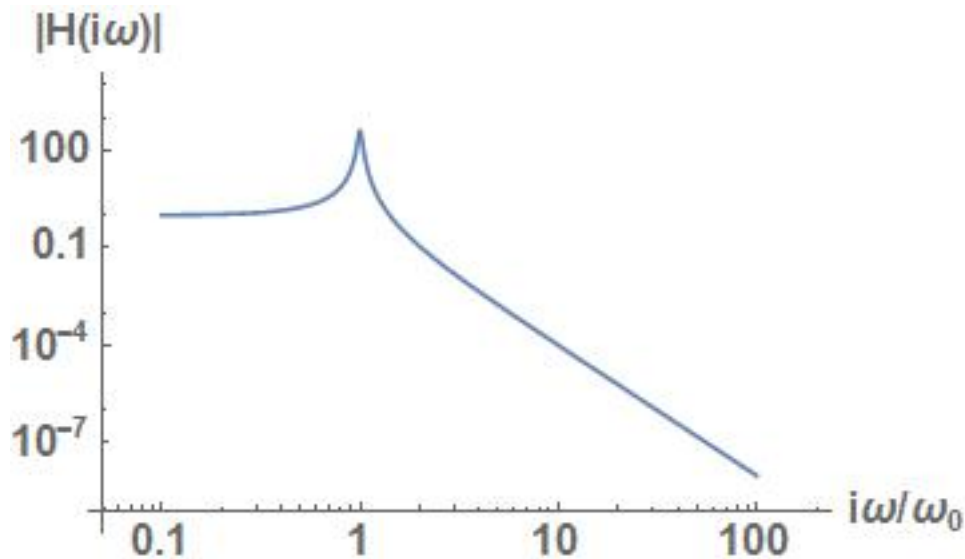


Figure 1: Oscillator Transfer Function

The quality factor Q of the resonator is defined as $Q = \omega_0/\Delta$, where Δ is the full width half max of the transfer function peak. From this definition, we have:

$$Q = \omega_0/\gamma = \frac{\omega_0\tau}{2} \quad (5)$$

The impulse response of the system can be found by taking the inverse Laplace transform of the transfer function:

$$x(t) = e^{-t/\tau} \sin(t\sqrt{\omega_0^2 - \gamma^2/4}) \quad (6)$$

where again the γ^2 term can be safely ignored, so the final form of the impulse response is:

$$x(t) = e^{-t/\tau} \sin(\omega_0 t) \quad (7)$$

This is simply a damped sinusoid, and an example trace of an underdamped oscillator is shown below:

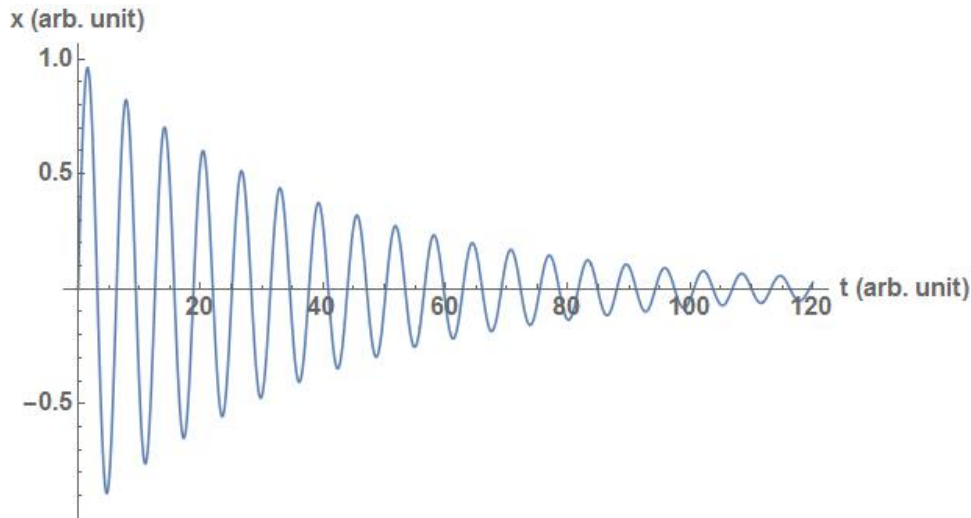


Figure 2: Oscillator Impulse Response

3 Internal Damping

Equation 1 is not the only way to model a damped system. Internal damping within materials is frequently described using a complex spring constant k [4]. In this model, the equation of motion becomes:

$$m\ddot{x} + k(1 + i\phi)x = f_{ext} \quad (8)$$

where $\phi(\omega)$ is called the loss angle. The loss angle represents the phase lag between a sinusoidal restorative force and the resulting sinusoidal displacement. It can be shown that the oscillator loses a fraction $2\pi\phi$ of its kinetic energy per cycle by intergrating the work done by the restorative force over a single displacement period. Again taking the Laplace transform and setting the two different parametrizations equal to each other yields the expression:

$$\gamma(\omega) = \frac{\omega_0^2\phi}{\omega} \quad (9)$$

The quality factor is only defined on resonance $\omega = \omega_0$, so:

$$Q = \frac{1}{\phi(\omega_0)} = \frac{\omega_0 \tau}{2} \quad (10)$$

This relationship forms the motivation for studying the decay time τ of the oscillator. By measuring τ we can calculate the loss ϕ , which then tells us about the thermal noise of the resonator through the fluctuation-dissipation theorem.

4 Experimental Setup

Our lab has two vacuum chambers used for testing resonators. The smaller chamber is used as a prototyping stage where quick testing can be performed on new cantilever designs. The larger chamber is a cryostat used for making measurements at extremely low temperatures using liquid nitrogen and liquid helium. The cryostat also contains the electronics necessary for making continuous Q measurements.

The silicon cantilever is mounted on one end using a stainless steel clamp and the other end is driven using an electrostatic driver (ESD). Different clamps are used depending on the cantilever geometry. The cantilever displacement is measured by sending a HeNe laser beam through a window in the cryostat. After the beam is reflected off of the cantilever, it returns to a calibrated quadrant photodiode which measure the position of the beam which is proportional to the cantilever displacement. Additional components in the system include a power resistor used to control resonator temperature and a polyether ether ketone (PEEK) base underneath the clamp for insulation from the cold plate. A SolidWorks model of the experimental setup is shown below:

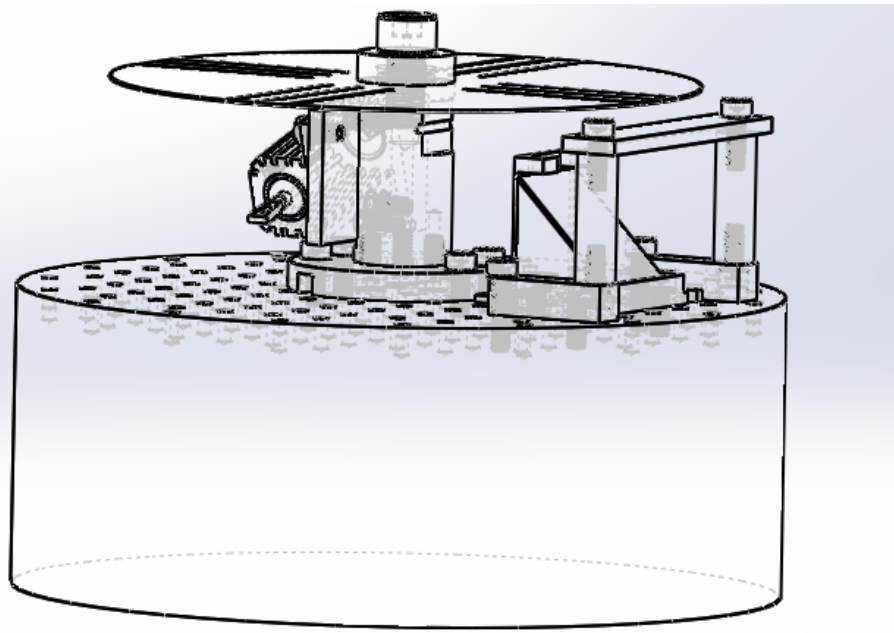


Figure 3: SolidWorks Experiment Model

The following picture shows a different clamp used for rectangular cantilevers.

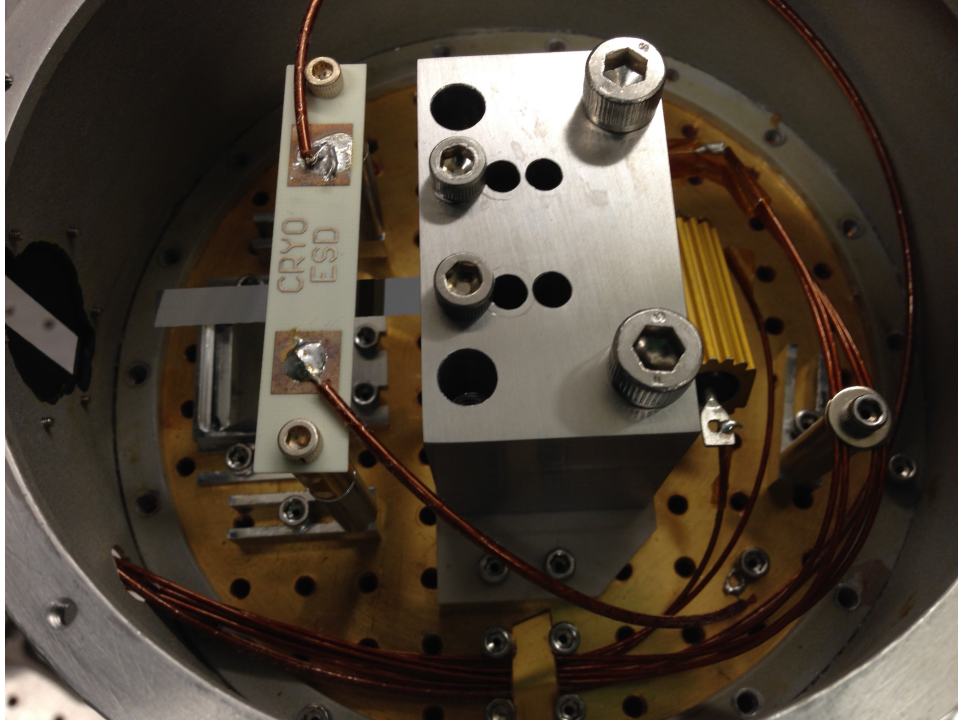


Figure 4: Actual Experimental Assembly

5 Cantilever Designs

We focus our analysis on three silicon cantilever designs. The first is a Glasgow-style cantilever received from a group in Taiwan. Previous measurements indicate that this is the highest quality resonator of the three, most likely due to a combination of better wafer quality and geometry favorable for minimum clamping loss. The dimensions are shown below:

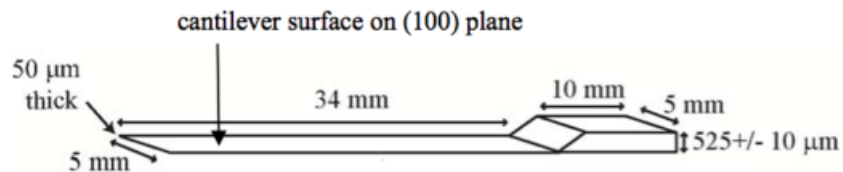


Figure 5: Taiwan Cantilever

We also study a barbell-style cantilever which has a rectangular shape with a thinner section

in the middle:

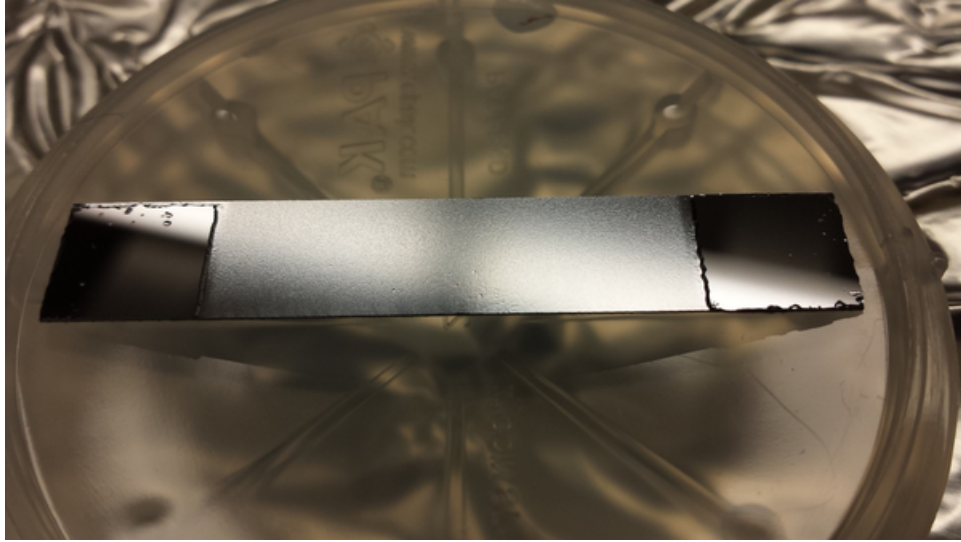


Figure 6: Painter2 Cantilever

The entire cantilever is 5cm long and 1cm wide. The two thicker end sections have a thickness of $650\mu\text{m}$ and the thinner middle section is $250\mu\text{m}$ thick. The inner section was etched using a piranha solution. Both the Taiwan and Painter2 resonators are mounted in a rectangular clamp.

Lastly we have a pinwheel style resonator that has four cantilever arms of different lengths. This resonator is mounted on a radially symmetric post for measurements. All dimensions shown below are in inches:

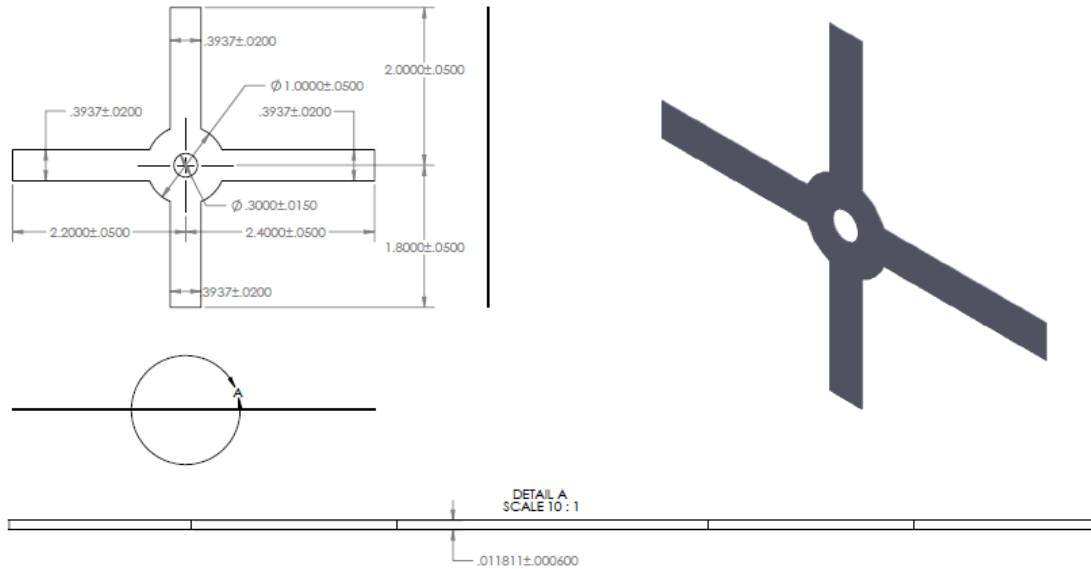


Figure 7: Pinwheel Cantilever

6 Measurement Techniques

6.1 Ringdown Method

In the ringdown experiment we determine the Q factor and loss angle of a thin silicon cantilever by measuring the time constant τ of a damped sinusoidal amplitude signal. The general data analysis procedure consists of taking a fourier transform of the amplitude signal and then bandpass filtering around the resonant frequency of the oscillator. An exponential curve can then be fitted to the filtered time domain signal in order to estimate the decay time τ . Several plots outlining this procedure are shown in Figure 8 below:

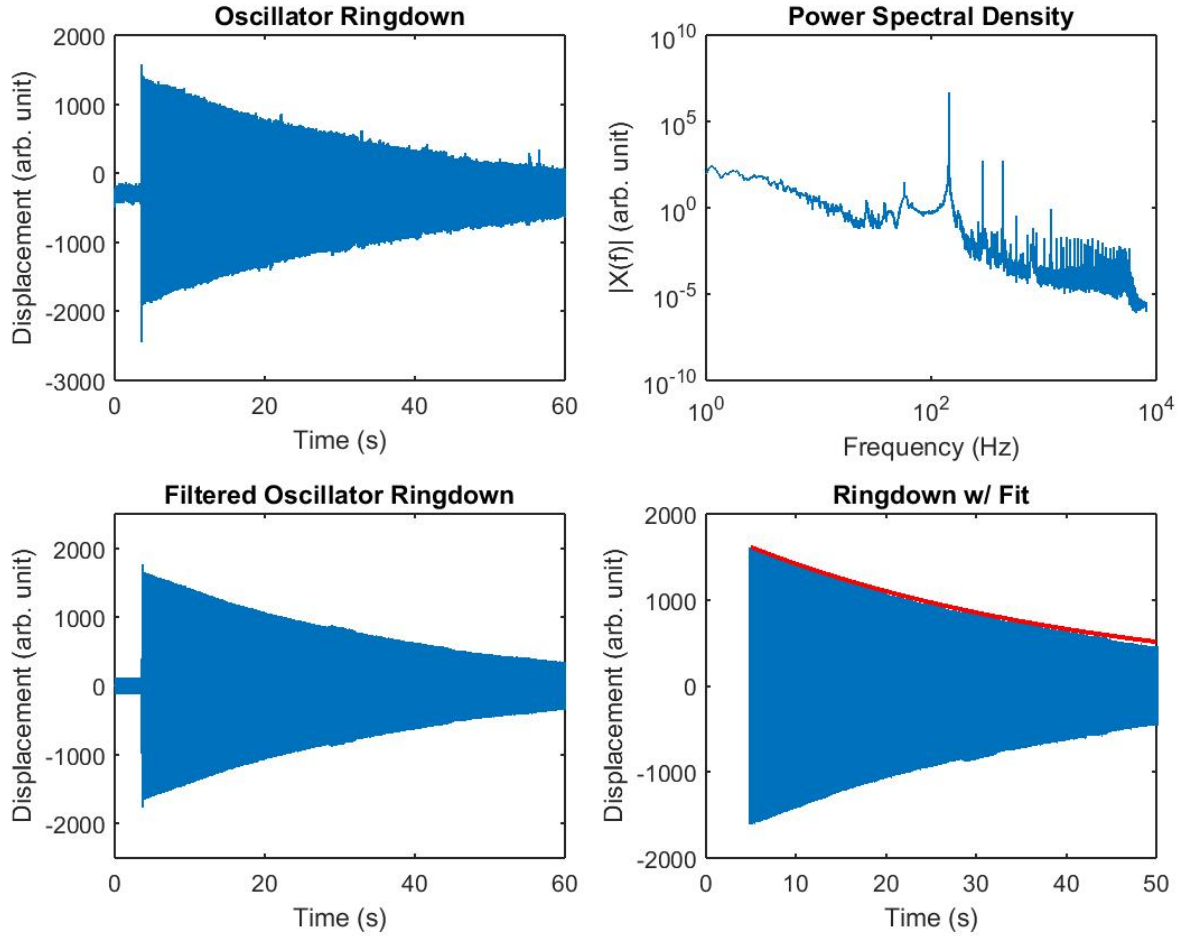


Figure 8: Data Analysis Procedure. Cantilever displacement data is taken from a quadrant photodiode and bandpass filtered around the resonant mode frequency. An exponential curve is then fit to the filtered data in order to estimate the characteristic decay time τ .

In the example analysis above, the Q was determined to be $\approx 17,755$ with $\omega_0/2\pi = 143.9\text{Hz}$. This measurement was performed on the fundamental Painter2 cantilever mode at room temperature.

6.2 Continuous Method

In addition to the ringdown method described above, we also utilize a previously developed continuous measurement technique to calculate the Q of our resonators. The continuous measurement technique employs more advanced control systems such as a phase-locked loop (PLL) and amplitude-locked loop (ALL) in order to drive the oscillator under test (OUT) at a constant amplitude. A simple block diagram of the system is shown below:

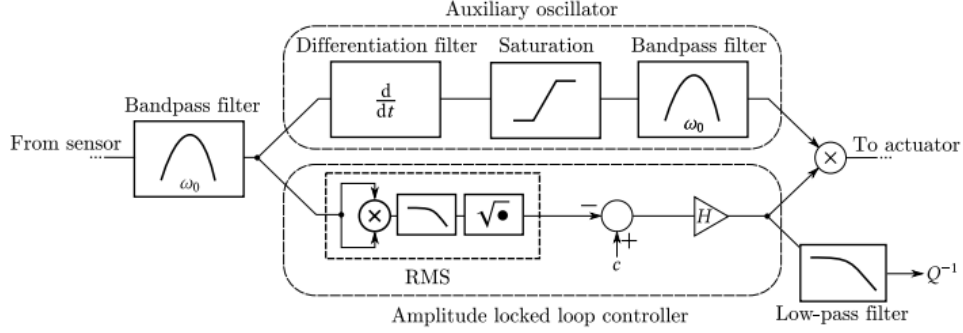


Figure 9: Continuous Measurement Block Diagram

A quadrant photodiode acts as the sensor in our current setup, measuring the relative displacement of the cantilever. From this signal we bandpass filter around the modes resonant frequency ω_0 and send the signal to the ALL and PLL. The PLL first differentiates the signal, producing a 90 degree phase shift. The signal is then amplified and sent through a saturation block where it becomes a square wave. Finally the signal is again bandpass filtered around ω_0 to produce a constant amplitude sine wave phase shifted 90 degrees ahead of the original displacement signal. The ALL works by taking the root mean square of the displacement signal and comparing the result to an amplitude set point c . The resulting error signal is then amplified by gain H and mixed with the PLL output to produce a drive signal for the actuator.

In the limit of high open loop gain where $\omega_U \gg \tau^{-1}$ it can be shown that [6]:

$$\phi = Q^{-1} = \frac{2\omega_U}{cH_U\omega_0} \langle a \rangle \quad (11)$$

Where a is the control output of H , $\omega_U = \frac{|SH_U A|}{2\omega_0}$ is the unity gain frequency (UGF), and H_U is the feedback gain evaluated at the UGF. Angle brackets indicate a time average. The frequency ω_0 can be easily calculated and the remaining parameters can be measured from information required to maintain the control loops.

This measurement technique allows for a continuous measurement of the Q of the resonator, which naturally allows for other parameters such as temperature or amplitude to be swept during the measurement process in order to determine the effect on ϕ . These are important factors when considering clamp design and isolation schemes. It can also be shown that measurements using this technique have a constant signal-to-noise ratio (SNR) since the oscillator is held at a constant amplitude, while the SNR decreases over time with the ringdown method. The continuous method is also useful for measuring very high Q oscillators, where the ringdown decay time may be impractical if not impossible to measure directly.

We have demonstrated the ability to measure different modes simultaneously using this method. However, we are often limited by the actuator gain A due to the physical setup of the experiment. The placement of our actuator, the ESD, heavily influences the modes we are able to excite based on how close the nodes of the particular mode are to the ESD active area. We are also unable to significantly excite torsional modes.

7 Mechanical Losses in Silicon

Mechanical losses in solids come from a variety of different dissipation mechanisms. These include processes such as phonon-phonon loss, surface loss, thermoelastic loss, and bulk loss. We expect thermoelastic loss and surface loss to be significant loss mechanisms due to our silicon resonator geometry. Various other dissipation processes such as gas damping are inevitably present in our system, but should be negligible compared to other losses.

7.1 Thermoelastic Loss

Thermoelastic loss occurs when a solid is bent. As certain local regions are compressed they heat up, while stretched regions are cooled (assuming a positive coefficient of thermal expansion). This creates temperature gradients in the material. Heat fluxes driven by the temperature gradient irreversibly dissipate energy, thus causing loss. Since thermoelastic loss is highly dependent on the material coefficient of thermal expansion, cryogenic silicon naturally becomes a good material choice for high quality mechanical systems due to its vanishing coefficient of thermal expansion at 124K.

For isotropic materials in pure bending modes, the thermoelastic loss ϕ_{TE} is given by the equation [5]:

$$\phi_{TE} = \frac{\alpha^2 Y T}{\rho C_p} \frac{\omega \tau}{1 + \omega^2 \tau^2} \quad (12)$$

where α is the coefficient of thermal expansion, Y is Young's modulus, T is the temperature, ρ is the material density, C_p is the heat capacity, and ω is the angular frequency of the particular bending mode. The additional time constant τ is defined as:

$$\tau = \frac{\rho C_p t^2}{\pi \kappa} \quad (13)$$

where t is the thickness of the resonator and κ is the thermal conductivity. Figure 10 below shows several plots of the thermoelastic loss as a function of temperature and angular frequency. A thickness $t = 50\mu m$ is assumed:

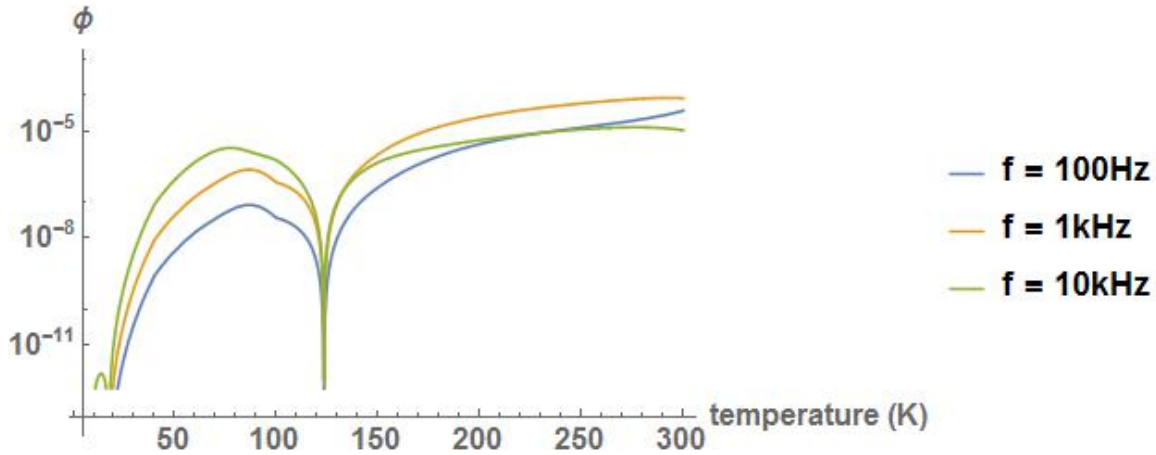


Figure 10: Thermoelastic Loss as a function of temperature and mode frequency. The sharp drop in ϕ at $T = 124\text{K}$ corresponds to when α , the thermal expansion coefficient of silicon, goes to zero.

Using [12](#), we predict a $Q \approx 50,000$ for rectangular cantilevers close to our geometry. This value is much higher than both our experimental data and COMSOL FEA modeling which are shown below, indicating that thermoelastic loss probably isn't the limiting factor in our system.

Table 1: Thermoelastic Loss in Silicon Pinwheel

Pinwheel Arm Length	Eigenfrequency (Hz)	Q (ringdown method)	COMSOL Predicted Q
2.4''	184	2,260	29,583
2.2''	228	—	23,103
2.0''	294	2,300	17,995
1.8''	392	1,000	12,875

The COMSOL predicted Q is much lower than the theoretical equation because the COMSOL model also considers thermoelastic loss in the clamp and washers. Thermoelastic loss was modeled in COMSOL by simulating temperature gradients caused by stretching and squeezing in the cantilever. An example of temperature analysis is shown below using the fundamental mode of the Painter2 cantilever:

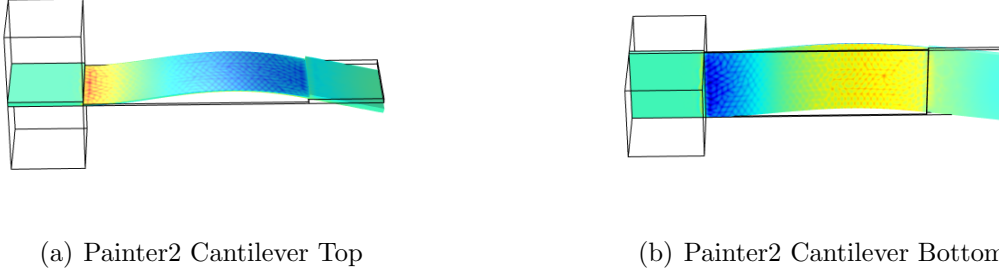


Figure 11: The models above represent relative heating in the cantilever, from which thermoelastic loss is calculated. Red represents warmer, compressed regions while blue represents cooler, stretched regions.

7.2 Clamp Design and Clamp Loss Simulations

We are never truly measuring the cantilever loss in any of our experiments because the cantilever isn't a closed system fixed to an infinitely stiff anchor. Our measured loss is an aggregate of losses in the cantilever, clamp, PEEK base, and even the cyrostat itself. Losses in the clamp have been significant in previous experiments, so optimizing the clamp design to minimize loss is an important task. The ϕ we actually measure can be estimated with the equation:

$$\phi_{measured} \approx \phi_{Si} + \frac{E_{clamp}}{E_{total}}\phi_{clamp} + \frac{E_{PEEK}}{E_{total}}\phi_{PEEK} + \dots \quad (14)$$

Where E is the total strain energy stored in the particular component. This formula provides a useful criterion for estimating the merit of new clamp designs.

A new clamp model was recently designed for the next series of quality factor measurements. Major changes from the previous model include a much thicker diameter and a lip to constrain the sapphire washers and pinwheel cantilever itself in an effort to decrease clamp loss. The design can be seen below:

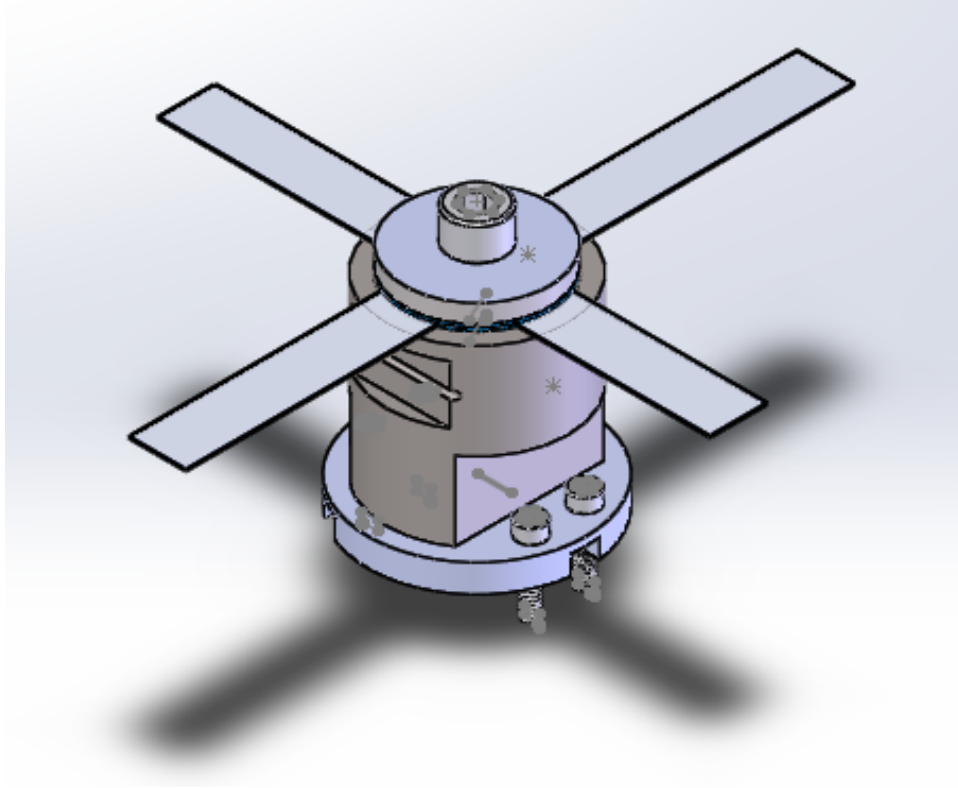


Figure 12: New Clamp Design

In order to test the new clamp design we created a COMSOL model of the system to calculate the strain energy stored in each component for the first several modes of the longest (2.4in) pinwheel cantilever. The model and results are displayed below:

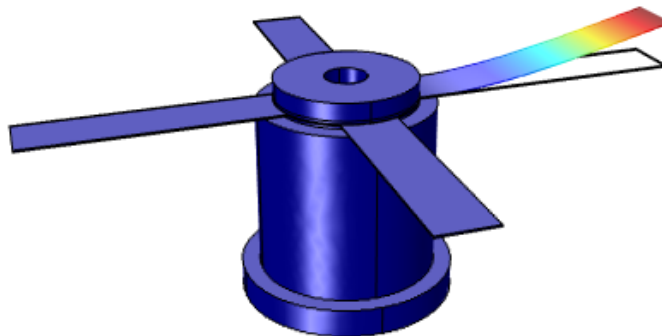


Figure 13: COMSOL Model of 2.4" Cantilever, Fundamental Mode

Table 2: Elastic Strain Energy Ratio

Eigenfrequency (Hz)	$E_{pinwheel}$ (arb. unit)	E_{clamp} (arb. unit)	Ratio
161	3016	3.4	1.1e-3
1009	120264	139	1.2e-3
1449	212434	160	0.8e-3

The low strain energy ratios indicate that energy leakage into the clamp shouldn't be a significant factor in our measurements.

7.3 Surface Loss

Surface loss effects might also be a significant contribution to the net loss of our resonators. These effects are not well understood and may be influenced by things like surface roughness, local lattice imperfections, and thin film deposits from other materials. We experimented with surface loss simulations in COMSOL by adding thin, lossy layers to the surface of our cantilever models. The following table shows the computational results of adding $19\mu\text{m}$ lossy surface layers to the 2.4in pinwheel arm, along with experimental data:

Table 3: Surface Loss in Silicon Pinwheel

Eigenfrequency (Hz)	Q (ringdown method)	Bulk Loss	Surface Loss	COMSOL Predicted Q
161	2,260	2e-5	9e-4	2,230
1009	1,260	1e-4	9e-4	2,044
1449	3,600	8e-6	9e-4	2,280

These simulations closely match our experimental results and may indicate that there is considerable surface loss in our system. With these results in mind, we imaged the surface of the Taiwan cantilever using a USB microscope.

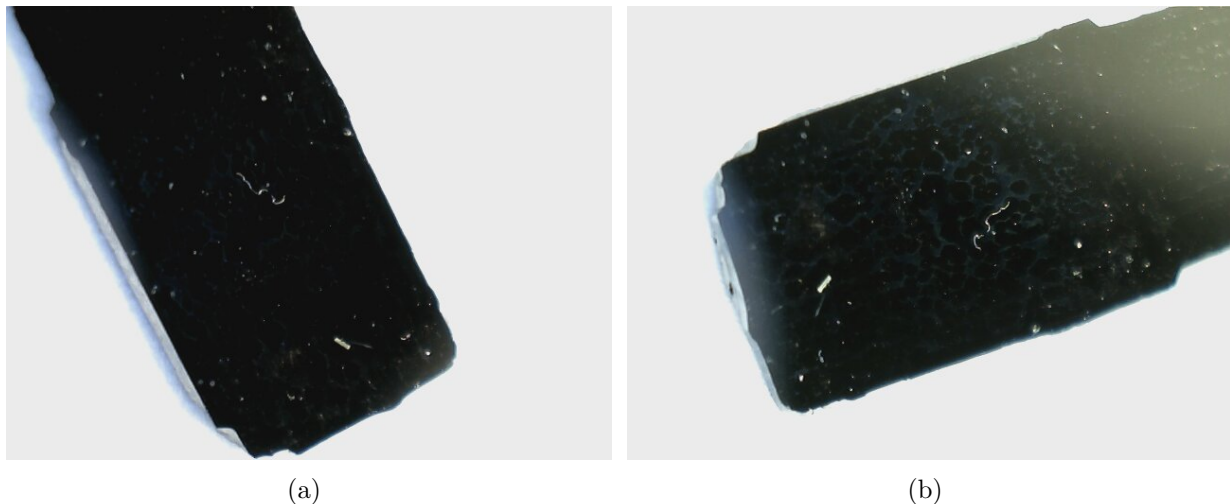


Figure 14: Taiwan Cantilever Surface

Although it is difficult to make quantitative observations, it is clear that the cantilever surface is not perfectly smooth. In an effort to improve the appearance of the surface, we cleaned the cantilever with isopropyl and again imaged the surface.



Figure 15: Cleaned Taiwan Cantilever Surface

Large surface imperfections are clearly visible even after the cleaning. While there are no immediate remedies for this problem, these results do indicate that we may be limited by lossy surface effects. Surface deformities also appear to grow worse over time since we tend to measure a decreasing Q the more we handle and reclamp the cantilevers. We will continue to explore better manufacturing, etching, and cleaning techniques in order to minimize surface losses.

8 Future Work

We are going to continue adjusting the continuous Q measurement system until we are able to reliably and robustly measure the Q of the first several oscillator modes simultaneously. This will involve tweaking control parameters and implementing additional filtering so that mode coupling is minimized.

The temperature sensor in the cryostat has recently been brought back into commission. With the sensor functional we will be able to accurately measure the Q of our cantilevers at cryogenic temperatures. This will be especially useful in determining whether or not we are limited by thermoelastic loss.

A larger cryogenic experiment is also currently under construction. Once the optimal silicon flexure design has been attained, it will be incorporated into the other experiment. The goal of this larger experiment is to directly measure the thermal noise in thin silicon structures by locking a laser to two separate cavities. Each cavity consists of a static mirror and a mirror attached to a silicon structure. Thermal noise can then be measured interferometrically by looking at the beat note formed by the two locked laser beams. The experiment is well into assembly; most optical and electronic systems have been set up.

List of Figures

1	Oscillator Transfer Function	3
2	Oscillator Impulse Response	4
3	SolidWorks Experiment Model	5
4	Actual Experimental Assembly	6
5	Taiwan Cantilever	6
6	Painter2 Cantilever	7
7	Pinwheel Cantilever	8
8	Data Analysis Procedure. Cantilever displacement data is taken from a quadrant photodiode and bandpass filtered around the resonant mode frequency. An exponential curve is then fit to the filtered data in order to estimate the characteristic decay time τ	9
9	Continuous Measurement Block Diagram	10
10	Thermoelastic Loss as a function of temperature and mode frequency. The sharp drop in ϕ at $T = 124\text{K}$ corresponds to when α , the thermal expansion coefficient of silicon, goes to zero.	12
11	The models above represent relative heating in the cantilever, from which thermoelastic loss is calculated. Red represents warmer, compressed regions while blue represents cooler, stretched regions.	13
12	New Clamp Design	14
13	COMSOL Model of 2.4" Cantilever, Fundamental Mode	14
14	Taiwan Cantilever Surface	15
15	Cleaned Taiwan Cantilever Surface	16

List of Tables

1	Thermoelastic Loss in Silicon Pinwheel	12
2	Elastic Strain Energy Ratio	15
3	Surface Loss in Silicon Pinwheel	15

References

- [1] A.V. Cumming, L. Cunningham, G. D. Hammond, K. Haughian, J. Hough, S. Kroker, I. W. Martin, R. Nawrodt, S. Rowan, C. Schwarz, and A. A. van Veggel, *Silicon mirror suspensions for gravitational wave detectors*. Quantum Grav. 31 025017 (2013).

- [2] Edward Taylor, Nicolas Smith, *Quality Factor of Crystalline Silicon at Cryogenic Temperatures*. LIGO Document P1300172-v1 (2013).
- [3] Marie Lu, Nicolas Smith, Rana Adhikari, Zach Korth, *Measuring the Quality Factor of Cryogenic Silicon*. LIGO Document T1400668-v1 (2014).
- [4] P.R. Saulson, *Thermal Noise in mechanical experiments*. Phys. Rev. D 42, 2437 (1990).
- [5] R. Nawrodt, C. Schwarz, S. Kroker, I. W. Martin, F. Brckner, L. Cunningham, V. Groe, A. Grib, D. Heinert, J. Hough, T. Ksebier, E. B. Kley, R. Neubert, S. Reid, S. Rowan, P. Seidel, M. Thrk, A. Tnnermann, *Investigation of mechanical losses of thin silicon flexures at low temperatures*. Quantum Grav. 30, 115008 (2013).
- [6] Nicolas Smith, *A technique for continuous measurement of the quality factor of mechanical oscillators*. Review of Scientific Instruments 86, 053907 (2015); doi: 10.1063/1.4920922